

MIXED CONVECTION IN POISEUILLE FLUID FROM AN ASYMMETRICALLY CONFINED HEATED CIRCULAR CYLINDER

by

Housseem LAIDOUDI* and Mohamed BOUZIT

Laboratory of Science and Naval Engineering (LSIM), Faculty of Mechanical Engineering,
USTO-MB, Oran, Algeria

Original scientific paper
<https://doi.org/10.2298/TSCI160424172L>

This paper examines the effects of thermal buoyancy on momentum and heat transfer characteristics of symmetrically and asymmetrically confined cylinder submerged in incompressible Poiseuille liquid. The detailed flow and temperature fields are visualized in term of streamlines and isotherm contours. The numerical results have been presented and discussed for the range of conditions as $10 \leq Re \leq 40$, Richardson number $0 \leq Ri \leq 4$, and eccentricity factor $0 \leq \varepsilon \leq 0.7$ at Prandtl number $Pr = 1$, and blockage ratio $B = 20\%$. The representative streamlines and isotherm patterns are presented to interpret the flow and thermal transport visualization. When the buoyancy is added, it is observed that the flow separation diminishes gradually and at some critical value of the thermal buoyancy parameter it completely disappears resulting a creeping flow. Additionally, it is observed that the down vortex requires more heating in comparison to upper vortex in order to be suppressed. In the range $1.5 \leq Ri \leq 4$, two counter rotating regions appear above the cylinder and on the down channel wall behind the cylinder. The total drag coefficient, C_D , increases with increasing Richardson number at ($\varepsilon = 0$). Moreover, an increase in eccentricity factor from 0 to 0.3 increases C_D by 37% at $Re = 10$, and 30% at $Re = 20$ for $Ri = 4$. An increase in eccentricity factor form 0 to 0.4 increases local Nusselt number by 20.4% at $Re = 10$, and 18.6% at $Re = 30$ for $Ri = 4$.

Key words: *steady flow, thermal buoyancy, asymmetrically cylinder, Nusselt number, flow separation, drag coefficient, mixed convection, Richardson number*

Introduction

Flow pattern and its characteristics around immersed bluff bodies have been studied by many researches because of the complexities and practical importance of these flows, the principle issues of classical flow configuration are wake formation, flow separation, the external forces acting on the body (drag and lift), and especially the heat transfer rate changing among the fluid-flow and the immersed body. The results show that the flow over a cylinder depends on large number of parameters and geometrical shapes such as type of fluid-flow (compressible or incompressible, Newtonian or Non Newtonian) [1-4], confined or unconfined cylinder [5, 6], and symmetrically or asymmetrically confined cylinder [7-9]. Forced convection and fluid-flows over circular cylinder arise in many micro-channels, nuclear. Lots of detailed information exists on the forced convection and fluid-flow past a circular cylinder [10-16].

* Corresponding author, e-mail: hichemsoft19@gmail.com

Dhiman *et al.* [3] numerically investigated the effect of blockage ratio ($B = 1/8, 1/6, 1/4$) on the cross flow of power-law fluids over a square cylinder confined in channel for the range of values of the power-law index $0.5 \leq n \leq 2$, and Reynolds number range $1 \leq Re \leq 45$. Using 2-D unsteady forms of governing equations. The results showed that, for $10 \leq Re \leq 45$ the length of re-circulation zone is seen to increase almost linearly with Reynolds number and/or the power law index and to decrease with increasing blockage ratio for $B = 1/8$ and $1/6$. However, an opposite trend of non-dimensional re-circulation length can be observed for $B = 1/4$. So it can be considered $B = 1/5$ as a critical blockage ratio.

Rashidi *et al.* [17] carried out a convective heat transfer of Al_2O_3 -water nanofluid over an equilateral triangular obstacle to determine the optimum conditions for maximum heat transfer and the minimum drag coefficient. The computation simulations are done for different Reynolds number $1 \leq Re \leq 180$, solid volume fraction (0 to 0.05) and orientations of the triangular obstacle (0 to 60°). Also, a comparison is performed between the results of CFD analysis and Response surface methodology. It is found that the minimum drag coefficient is occurred at the degree 35.13° , $Re = 97.6$ and solid volume fraction 0.01, the maximum Nusselt number is found at the degree 8.49° , $Re = 180$ and solid volume fraction 0.005.

Rashidi and Esfahani [18] studied the effect of magnetic on forced convection heat transfer in a channel with a built-in square obstacle. The governing equations with the boundary conditions are solved using a finite volume method. The computation were done for fixed blockage ratio ($B = 1/8$) at $Pr = 0.71$ and Reynolds and Stuart (N) number ranging from 1 to 250 and 0 to 10, respectively. The results revealed that the existence of channel walls decreases the effects of magnetic field on Nusselt number.

Bovand *et al.* [19] simulated the forced convection heat transfer of Al_2O_3 -water nanofluid over an equilateral triangular obstacle with different orientations. The governing equations have been solved using finite volume method in the range of conditions: Reynolds number (1-200), solid volume fraction (0-0.05), the results showed that the required Reynolds number for wake formation decrease with increase in solid volume fraction.

The flow pattern even becomes more complicated when the boundary-layer separations are further influenced by heat transfer. It should be mentioned that for the low to moderate Reynolds number, the thermal buoyancy effect can significantly muddle the flow field [20-22]. The principal parameter that controls a relative effect of buoyancy is the Richardson number, defined as $Ri = Gr/Re^2$, where, Gr is the Grashof number, and Re is the Reynolds number. This number determines the relative importance of forced and natural convection. The free convection dominates over the forced convection when $Ri > 1$, and the forced convection dominates when $Ri < 1$. Both the free and forced convection dominate equally when Richardson number is nearly approached to 1.

Over the years, significant studies are now available in literature on the flow field and heat transfer around confined cylinder under the impact of cross-buoyancy, but are all limited to symmetrically cylinder. For that purpose, in this study, an attempt has been made to fill this gap for the confined flow around asymmetrically circular cylinder under aiding the thermal buoyancy mixed convection, at low Reynolds number.

Sarkar *et al.* [21] numerically investigated the combined effect of Prandtl number and Richardson 0 to 2 and for Reynolds number limited between 80-180, on the unsteady wake dynamic and heat transfer past symmetrically circular cylinder, using a streamline upwind/Petrov-Glerkin (SUPG) finite element method based finite element method to solve the governing equations, the results showed that the average Nusselt number decreases with increase Richardson number. Sukesan *et al.* [22] studied the effect of aiding thermal

buoyancy on flow field and heat transfer of a symmetrical semi-circular cylinder in horizontal channel under these range of conditions $Re = 1-40$, $Ri = 0-4$, $Pr = 0.71-50$, and blockage ratio 16.65% to 50%, the obtained results have found that the drag coefficient increases with increasing in Richardson number and/or blockage ration, the average Nusselt number increases with increase in Prandtl number, Also the average Nusselt number increase with increase in Richardson number. But it is still unknown about the effect of buoyancy strength on flow separation behind the cylinder at low Reynolds number. Chatterjee and Amiroudine [23] carried out a numerical simulation to understand the effect of thermal buoyancy over two equal isothermal square cylinders, the space between cylinders is fixed with four widths of cylinder, the finite volume method have been used to solve the governing equations in unsteady regime, the results are presented in the following conditions: $Re = 1-30$, $Pr = 0.7-100$, $Ri = 0-1$. It is found that the flow is completely steady for the chosen range of condition.

From the critical evaluation of the pertinent available literature in this field, it is obvious that although there are some results for the mixed convection heat transfer analysis around cylinder placed confined within a horizontal channel, there is no reported work on the effect of buoyancy strength on the flow separation at low Reynolds number, also there is no reported work on the effect of asymmetric confinement on thermal buoyancy. For that purpose, this work aims to examine the role of superimposed thermal buoyancy on the momentum and heat transfer characteristics of symmetrically and asymmetrically confined cylinder situated between parallel walls, the results are presented and discussed for these conditions $10 \leq Re \leq 40$, $Pr = 1$, $0 \leq Ri \leq 4$, eccentricity factor $0 \leq \varepsilon \leq 0.7$ at fixed blockage ratio $B = 0.2$.

Problem statement and governing equations

Figure 1 describes the geometry of present problem. Consider a heated circular cylinder, which is located in off-center position of a long 2-D horizontal channel. Due to numerical considerations, the flow enters the channel with fully developed velocity profile with a maximum velocity of, u_{max} , and constant temperature, T_{in} , and passes the asymmetrically cylinder, whose surface is maintained at constant temperature, T_w . The length of confined cylinder is defined, d , the ratio of this length to the height of the channel, H , defines the blockage ratio, $B = 0.2$. The upstream and downstream distances of the computational domain are selected as: $L_u = 10d$, $L_d = 20d$. The position of cylinder is defined by the eccentricity factor ε , $\varepsilon = e/(H/2 - d/2)$. Obviously at $\varepsilon = 0$, the cylinder will be exactly at the center of the channel and at $\varepsilon = 1$ it will touch one of the walls (the down channel wall in this work). The dimensionless governing equations for this 2-D, laminar, incompressible flow with constant thermophysical properties along with Boussinesq approximation and negligible viscous dissipation can be expressed in the following conservative forms:

– continuity

$$\frac{\partial u}{\partial x} + \frac{\partial v}{\partial y} = 0 \quad (1)$$

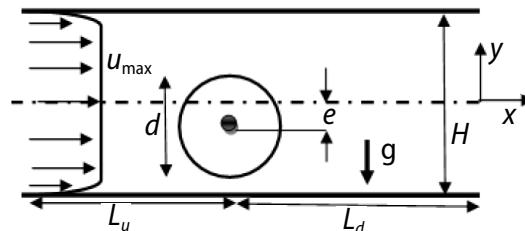


Figure 1. Geometry of the channel flow past an asymmetrically confined cylinder

– momentum

$$\frac{\partial uu}{\partial x} + \frac{\partial uv}{\partial y} = -\frac{\partial p}{\partial x} + \frac{1}{\text{Re}} \left(\frac{\partial^2 u}{\partial x^2} + \frac{\partial^2 u}{\partial y^2} \right) \quad (2a)$$

$$\frac{\partial uv}{\partial x} + \frac{\partial vv}{\partial y} = -\frac{\partial p}{\partial y} + \frac{1}{\text{Re}} \left(\frac{\partial^2 v}{\partial x^2} + \frac{\partial^2 v}{\partial y^2} \right) + \text{Ri} \theta \quad (2b)$$

– energy

$$\frac{\partial u\theta}{\partial x} + \frac{\partial v\theta}{\partial y} = \frac{1}{\text{Pr Re}} \left(\frac{\partial^2 \theta}{\partial x^2} + \frac{\partial^2 \theta}{\partial y^2} \right) \quad (3)$$

where u and v are the dimensionless velocity components along x - and y -directions of a Cartesian co-ordinate system, respectively, p – the dimensionless pressure, and $\text{Re} = (u_{\max} d/\nu)$ – the Reynolds number based on the cylinder dimension. The $\text{Ri} = \text{Gr}/\text{Re}^2$ – the Richardson number, $\text{Gr} = g\beta(T_w - T_{\text{in}})d^3/\nu^2$ – the Grashof number with g and β being the gravitational acceleration and volumetric expansion coefficient, respectively, θ – the dimensionless temperature, and $\text{Pr} = \nu/\alpha$ is the Prandtl number. The fluid properties are described by the density, ρ , kinematic viscosity, ν , and thermal diffusivity, α . The dimensionless variables are defined:

$$u = \frac{\bar{u}}{u_{\max}}, \quad v = \frac{\bar{v}}{u_{\max}}, \quad x = \frac{\bar{x}}{d}, \quad y = \frac{\bar{y}}{d}, \quad p = \frac{\bar{p}}{\rho u_{\max}^2}, \quad \theta = \frac{(T - T_{\text{in}})}{T_w - T_{\text{in}}} \quad (4)$$

The boundary conditions used for the flow and heat configurations are: at the inlet a fully developed velocity profile for laminar flow with a constant temperature, this is given by:

$$u = 1 - (|2By|)^2, \quad v = 0, \quad \theta = 0 \quad (5)$$

On the surface of the obstacle cylinder: the standard no-slip condition is used and the cylinder is maintained and heated with a constant temperature T_w .

$$u = 0, \quad v = 0, \quad \theta = 1 \quad (6)$$

At the channel walls, the usual no-slip condition for flow and adiabatic condition for energy are used.

$$u = 0, \quad v = 0, \quad \text{Adiabatic} \quad (7)$$

At the outlet Neumann boundary condition for field variables is employed:

$$\frac{\partial u}{\partial x} = 0, \quad \frac{\partial v}{\partial x} = 0, \quad \frac{\partial \theta}{\partial x} = 0 \quad (8)$$

The total drag coefficient, which is a combination of friction drag and pressure drag, is computed as follows:

$$C_D = \frac{2F_D}{\rho u_{\max}^2 d} \quad (9)$$

where F_D is the drag force on the surface of the circular cylinder, the local Nusselt number on the surface of the isothermal circular cylinder is evaluated using the temperature field:

$$\text{Nu} = \frac{hd}{k} = -\frac{\partial\theta}{\partial n_s} \quad (10)$$

Here h and n_s are the local surface heat transfer coefficient and the normal direction to the cylinder surface, respectively.

Numerical methodology

The governing fields eqs. (1)-(3), subjected to the aforementioned boundary conditions have been solved numerically using *ANSYS-CFX* version (14.0). This commercial code is a high performance, a general purpose fluid dynamics program that is capable of solving diverse and complex 3-D geometries. This code uses the governing equations to describe the principal processes of momentum, mass, and heat transfer. It also combines a specific number of mathematical models such as (power-law, k - ϵ ...) that can be used simultaneously with fundamental equations to describe other physical and chemical phenomena such as combustion, turbulence, *etc.* This present CFD package applies the finite volume method to convert the governing PDE into a system of discrete algebraic equations by discretizing the computational domain into grid mesh.

Choice of numerical parameters

In order to obtain reliable and accurate results, it is imperative to choose prudently the following parameters defining the flow domain: the grid size, upstream distance, L_u , and downstream distance, L_d , this section addresses these issues in some detail.

Grid independency study

The unstructured trilateral cells of non-uniform grid spacing were generated using the package *GAMBIT* (version 2.4.6). The grid points are distributed in a non-uniform manner with higher concentration near the cylinder as it is shown in fig. 2. In order to investigate the solution grid independency and to choose a reasonable mesh resolution. Grid independence test was carried out with respect to average values of Nusselt numbers and total drag coefficient, C_D , at Reynolds number of 10, and Richardson number of 0, three different meshes were generated viz. Mesh1, Mesh2, and Mesh3. Table 1 shows the meshes and corresponding numbers of elements used in this study. Here C_N is the numbers of nodes on the face of the cylinder. From tab. 1 it is evident that the average Nusselt number shows variation of 0.003%, and 0.002% whether total drag coefficient have 0.015 % and 0.010% with meshes Mesh1 and Mesh3. So for the present computations the grid-independent situation was established for Mesh2 which is computationally economical for all different cases studied in this present work. All the computations are carried out in an Intel (R) Core (TM) 2 Duo CPU T5870@2.0 GHz PC computer.

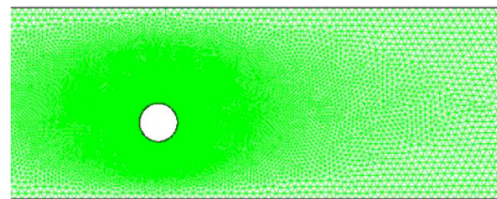


Figure 2. Mesh inside solution domain

Table 1. Effect of control volumes on C_D and Nu at Re = 10, Pr = 1, and Ri = 0

| Grid | Elements | C_N | Nu | P. D.% | C_D | P. D.% |
|-------|----------|-------|---------|--------|---------|--------|
| Mesh1 | 89278 | 250 | 2.26397 | 0.003 | 4.09664 | 0.015 |
| Mesh2 | 120358 | 300 | 2.26405 | 0.002 | 4.09729 | 0.010 |
| Mesh3 | 168624 | 400 | 2.26401 | – | 4.09774 | – |

Influence of upstream and downstream

The upstream and downstream distances of the computational domain were chosen based on the comprehensive studies on the effects of the finite domain on C_D and Nusselt number for symmetrically cylinder at Reynolds number ($Re = 10$), Prandtl number $Pr = 1$, and $Ri = 0$. Increasing the upstream L_u and downstream L_d distances made maximum differences in C_D and Nusselt number for $Re = 10$, $Pr = 1$, and $Ri = 0$. For this condition, the upstream distance of $L_u = 10d$ was chosen according to the changes in the values of C_D and Nusselt number for $L_u = 5d$, $10d$, and $15d$ when $L_d = 20d$ as shown in tab. 2. Furthermore, an increment in the downstream distance from 10 to 25 (for $L_u = 10d$) led to the minor percentage changes of less than 0.001% in the drag coefficients and the Nusselt number and hence the value of $L_d = 20d$ was used in this study.

Table 2. Effect of upstream, downstream distances on C_D , and Nu at $Re = 10$, $Pr = 1$, and $Ri = 0$

| L_u | C_D | P. D. [%] | Nu | P. D. [%] | L_d | C_D | P. D. [%] | Nu | P. D. [%] |
|-------|---------|-----------|---------|-----------|-------|---------|-----------|---------|-----------|
| 5d | 4.09875 | 0.003 | 2.2643 | 0.001 | 10d | 4.09707 | 0.006 | 2.26402 | 0.002 |
| 10d | 4.09731 | 0.001 | 2.26404 | 0.003 | 20d | 4.09731 | 0.001 | 2.26404 | 0.003 |
| 15d | 4.09694 | - | 2.26397 | - | 25d | 4.09695 | - | 2.26396 | - |

Validation test

The numerical solution procedure used herein has been validated by comparing the present values with the previous results on forced and mixed convection heat transfer from symmetrically square cylinder. For the forced convection test, the totals drag coefficient and average Nusselt number of cylinder in the range of $10 \leq Re \leq 40$ for $Pr = 50$ and $B = 0.25$ are

Table 3. Comparison of Nu and C_D for different values of Re for a square cylinder, $B = 1/4$

| Re | C_D | C_D [14] | Error [%] | Nu | Nu [14] | Error [%] |
|----|-------|------------|-----------|------|---------|-----------|
| 10 | 7.26 | 7.1 | 2.2 | 6.31 | 6.33 | 0.31 |
| 30 | 11.0 | 11 | 0.18 | 2.94 | 3.01 | 2.32 |
| 40 | 12.10 | 12.15 | 0.41 | 2.52 | 2.51 | 0.4 |

Table 4. Comparison of Nu for different values of Re, for a two square cylinders at $Ri = 0.25$

| Re | First cylinder | | | Second cylinder | | |
|----|----------------|---------|-----------|-----------------|---------|-----------|
| | Nu | Nu [23] | Error [%] | Nu | Nu [23] | Error [%] |
| 1 | 1.79 | 1.8 | 0.5 | 1.26 | 1.3 | 3 |
| 10 | 3.94 | 3.94 | 0 | 2.59 | 2.6 | 0.4 |
| 30 | 6.37 | 6.4 | 0.5 | 3.78 | 3.83 | 1.3 |

presented in tab. 3. A good agreement is seen between the results of present work and the results reported in the literature of Jahromi *et al.* [14], the maximum deviation is less than 2.5%. The second set of test is a mixed convection for Newtonian fluid-flow over two equal isothermal square cylinders placed in a tandem arrangement within a horizontal channel in the range of this condition as, $1 \leq Re \leq 30$, for $Pr = 10$, and $Ri = 0.25$. The computed results are presented in tab. 4. Again a good agreement is observed between predictive results and the results of [23], the maximum deviation is about 3%.

Results and discussion

Symmetrically cylinder

In this section, the influences of superimposed thermal buoyancy on flow field and heat transfer phenomena are presented, also some important dimensionless global hydrodynamic and thermal parameters such as drag coefficient, re-circulation length and Nusselt number are

provided for laminar incompressible Newtonian flow over a symmetrically circular cylinder ($\varepsilon = 0$) situated in a horizontal channel under cross buoyancy for the controlling parameters like Re , and Ri ranging from 10 to 40, 0 to 4, respectively, at fixed blockage ratio $B = 20\%$ and $Pr = 1$.

The flow patterns in the vicinity of a circular cylinder are presented in figs. 3-5 by streamlines contours for different values of Re , Ri , at $\varepsilon = 0$. For forced convection ($Ri = 0$), and $\varepsilon = 0$ (centerline position) as shown in fig. 3 as usual the flow separation is found to be symmetric about the centerline for all Reynolds number. A closed steady re-circulation consisting of twin symmetric steady vortices (upper and down) forms behind the object, the bubble size increases along the stream wise as well as transversal directions with Reynolds number.

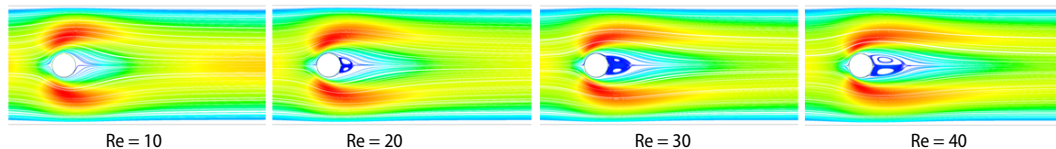


Figure 3. Streamlines around the cylinder for $Ri = 0$ (no thermal buoyancy), $\varepsilon = 0$ and $Pr = 1$ at different Reynolds numbers 10-40 (for color image see journal web site)

For mixed convection, fig. 4 shows the streamlines contours for Richardson number range of $Ri = 0-1$ at fixed $Re = 30$. From the fig. 4 the flow pattern loses its symmetry when thermal buoyancy is superimposed. However, the degree of asymmetry is increased with increase in the value of Richardson number. Furthermore, the flow separation behind the cylinder also becomes asymmetric and both separation points (upper, down) move toward the rear edge of the obstacle and accordingly, the re-circulation region progressively diminishes. Eventually, at some critical value of buoyancy parameter the flow does not separate at all behind the cylinder and above the critical buoyancy strength the flow creeps over the surface of cylinder. It is also shown that, the upper vortex suppresses more earlier than the down, this due to the fact that as Richardson number increases for constant Reynolds number, the velocity of fluid particles behind the cylinder increases and moves toward the upper channel wall, the inertia force is added with the viscous force, resulting in upper vortex delay first. Consequently, the incoming flow will be accelerated underneath the confined cylinder owing to the mass conservation principle, and this leads to increase the flow separation in the lower half of cylinder.

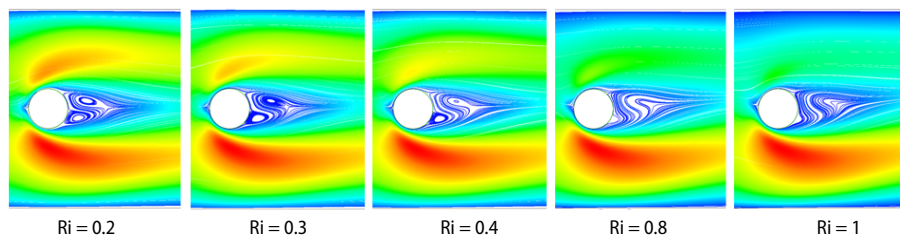


Figure 4. Streamlines around the cylinder for $Ri = 0.2-1$, $\varepsilon = 0$ and $Pr = 1$ at $Re = 30$ (for color image see journal web site)

Figure 5 shows streamlines for Richardson number range of $Ri = 1.5-4$, and for different Reynolds value. It is observed that, a counter rotating region forms above the cylinder. The region size increases along the stream wise as well as transverse directions with Re , and/or Ri , this behavior can be explained: above the value $Ri = 1$, the free convection dominates over forced

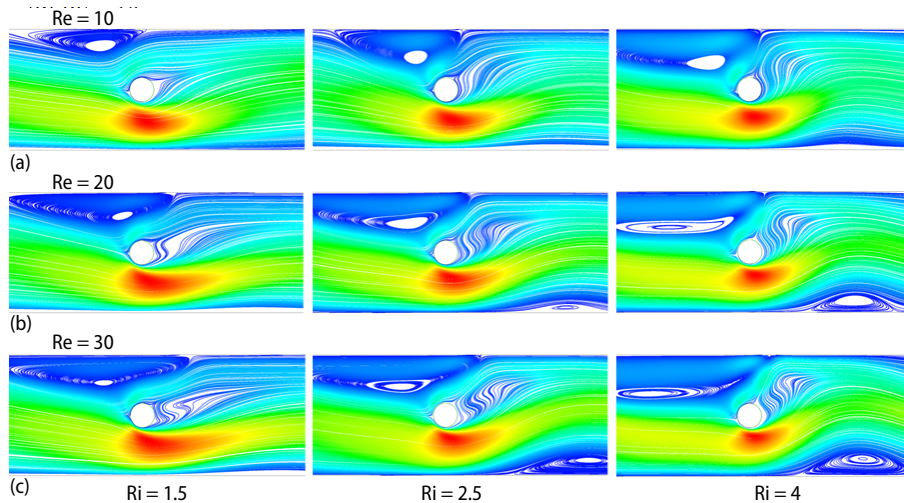


Figure 5. Streamlines around the cylinder for $Ri = 1.5-4$, $\varepsilon = 0$ and $Pr = 1$ at three $Re = 10, 20$ and 30 (for color image see journal web site)

convection. Accordingly, most fluid-flows below the cylinder. Hence, the mass-flow rate becomes more beneath the cylinder than above it which reversals the flow above the cylinder. Further, a wake region is also observed on the down channel wall behind the cylinder. This region is seen to be increased in stream wise and transversal directions by increasing the value of Re and/or Ri . It is due to the thermal buoyancy effect, which tows the flow toward the upper channel wall.

Figure 6, presents the quantitative variation of dimensionless vortex length of upper and down vortices behind the cylinder with Richardson number for $Re = 20$ and 30 . The re-circulation length for each vortex is a measure of the stream wise distance from the rear face of the obstacle to the re-attachment point for the near closed streamline along the vortex centerline, and it is defined as $L_R = \bar{L}_R / d$ where \bar{L}_R being the corresponding dimensional value of vortex length, it is clearly observed that at particle Reynolds number the re-circulation length of upper and down bubble are significantly reduced with increase in Richardson number. Moreover, the upper vortex is vanished earlier than the down. So these results substantiate what is previously explained.

Figure 7 presents the variation of total drag coefficient with Richardson number for different Reynolds number, From the fig. 7 it is found that the total drag coefficient decreases with increase in the Reynolds number due to the fact that, at low Reynolds number, the fluids el-

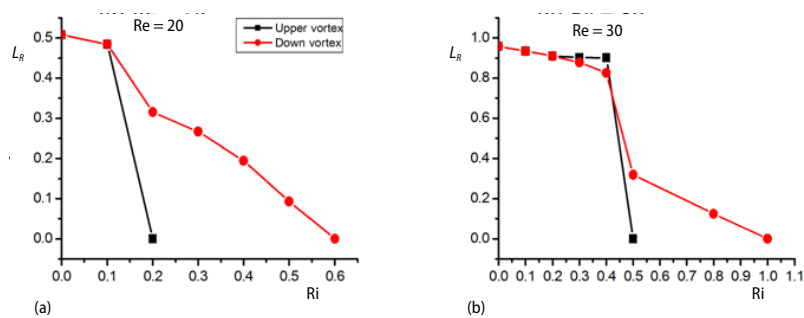


Figure 6. Variation of re-circulation length behind cylinder with Richardson numbers for different Reynolds numbers at $Pr = 1$

ement flow more closely to the cylinder than at the higher Reynolds number. Also, the viscous force decreases with increasing Reynolds number. Further, at fixed Reynolds number, the total drag coefficient increases with increase in Richardson number. This due to the fact that as Richardson number increases gradually from 0 to 1, more and more fluid comes to the bottom of the cylinders (as previously discussed) which results in a significant reduction of pressure at the top and behind cylinder and accordingly the drag coefficient increases. This effect is more pronounced when $Ri > 1$.

Figure 8 presents the variation of average Nusselt number on the circular cylinder with Richardson number for different Reynolds number. The surface average heat transfer is obtained by surface averaging the integral local Nusselt number along the cylinder surface. Figure 8 shows that the average Nusselt number increases as usual with the Reynolds number. Interesting variations are observed with respect to the Richardson number, for $Ri = 0-1$, the heat transfer rate increases slightly, and above the value 1, the average Nusselt number decreases, this may be due to the wake region that is appeared above the cylinder.

Asymmetrically cylinder

In this section, the effects of eccentricity factor and Richardson number on the flow pattern and heat transfer field around asymmetrically circular cylinder are introduced for different Reynolds number $10 \leq Re \leq 40$.

Figure 9 shows the streamlines for various eccentricity factor $\varepsilon = 0.2-0.7$, and $Ri = 1.5-4$ at $Re = 30$. It is observed that by increasing the eccentricity factor from 0.2 to 0.7

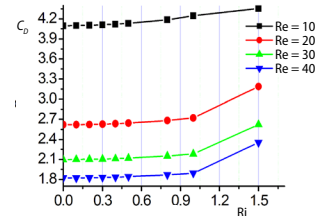


Figure 7. Variation of C_D with Ri for different Re , $\varepsilon = 0$ at $Pr = 1$

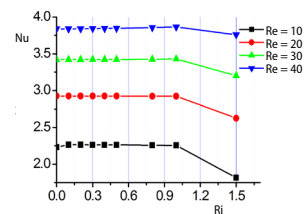


Figure 8. Variation of surface average cylinder Nusselt number with Ri for different Reynolds number

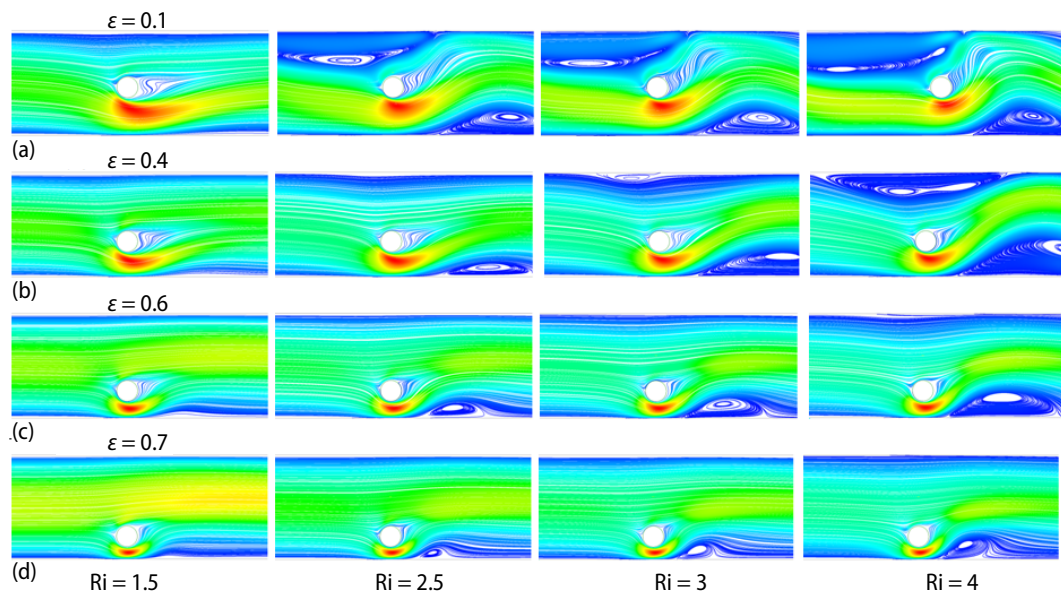


Figure 9. Streamlines around the cylinder for $Ri = 1.5-4$, $\varepsilon = 0.2 - 0.7$ and $Pr = 1$ at $Re = 30$
 (for color image see journal web site)

at fixed Richardson number, the wake region above the cylinder progressively diminishes both longitudinally as well as laterally, and the re-circulation center moves toward the stream-wise direction. Eventually, at some critical value of ε , the wake disappears at all above the obstacle. It is because of the mass-flow rate which is promoted over the cylinder. For the down wake, it is observed that the wake size increases in both directions with increase in eccentricity factor initially, and then again decreases. The elevation can be attributable to the fact that, in the case of asymmetric confinement, as expected, the fluid accelerates in the annular region between the cylinder and the lower wall, the local value of the Reynolds number is likely to be higher than its global value and this leads to increase the wake region.

One of the main parameter which affected by thermal buoyancy and eccentricity factor is drag coefficient. Figure 10 shows the dependence of the drag coefficient on the $\varepsilon = 0-7$ and $Ri = 0-4$ for different Reynolds number, $Re = 10-40$. In this figure, the values of C_D show the expected inverse dependence on Reynolds number. They also increase with an increase in the value of Richardson number. Figure 10 also shows that the values of C_D decrease as ε increases for $Ri = 0$ (forced convection). On other hand, in the range $0 < Ri \leq 1$, at fixed Reynolds number, generally the drag coefficient increases with increasing eccentricity factor, ε , then again decreases. For $1 < Ri \leq 4$, it is shown that depending upon the degree of asymmetry, the drag coefficient may increase or decrease thereby suggesting a non-monotonic relationship between the drag coefficient and asymmetric placement of cylinder. For example, an increase in eccentricity factor from 0 to 0.3 increases C_D by 37% at $Re = 10$, and 30% at $Re = 20$ for $Ri = 4$.

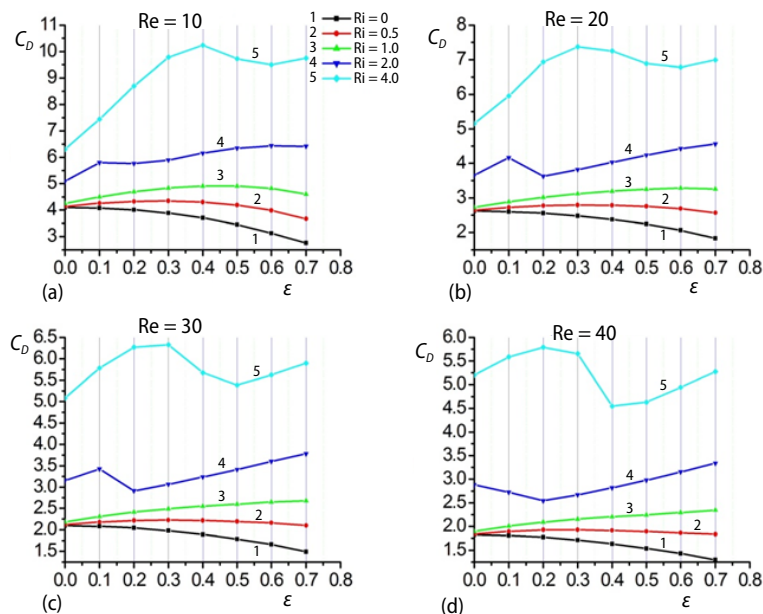


Figure 10. Effect of ε , Ri and Re on drag coefficient
(for color image see journal web site)

The isotherms around the circular cylinder for the range of Ri , ε , at fixed Reynolds number are depicted in fig. 11. The isotherms profiles are the reflection of physical phenomena observed from the analyses of streamlines patterns. More crowding of temperature contours is observed near to the curved surface of a circular cylinder compared to the flat surface, which results in a higher value of Nusselt number on the curved surface. The crowding of temperature

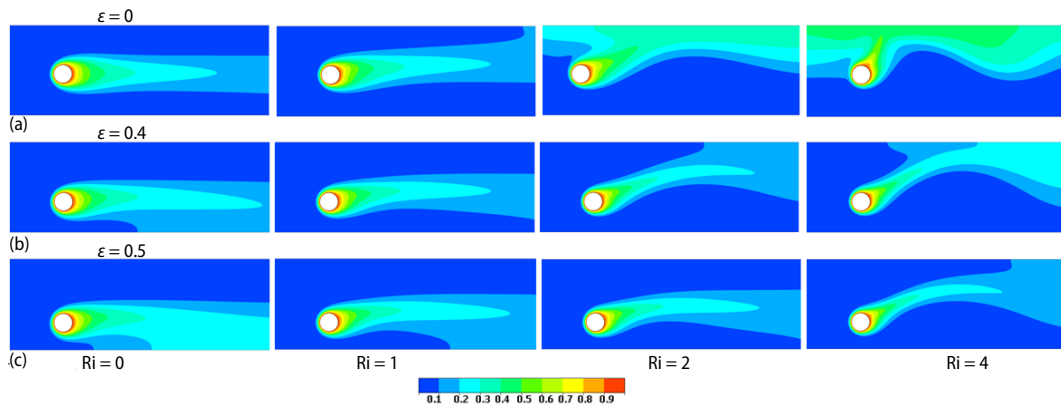


Figure 11. Isotherms around the cylinder for $Ri = 0-4$, $\varepsilon = 0.1$ and 0.3 and $Pr = 1$ at $Re = 30$
 (for color image see journal web site)

contours is found to be depended with Richardson number and eccentricity factor this result indicates that the heat transfer is depending with increasing Ri and/or ε . Like the streamlines patterns, the isotherm patterns become also asymmetric with the introduction of buoyancy and this asymmetry increases with increasing the strength of buoyancy *i. e.*, with higher Richardson number. Furthermore, the thermal buoyancy influences the flow on the rear surface much more than that on the other surfaces of the cylinder. Whereas increase in the value of eccentricity factor decreases the effect of thermal buoyancy on the flow behind the rear surface of cylinder.

Figure 12 presents the variation of average Nusselt number with eccentricity factor $\varepsilon = 0-0.7$ for different Richardson number, $Ri = 0-4$ and $Re = 10-40$ at fixed Prandtl number

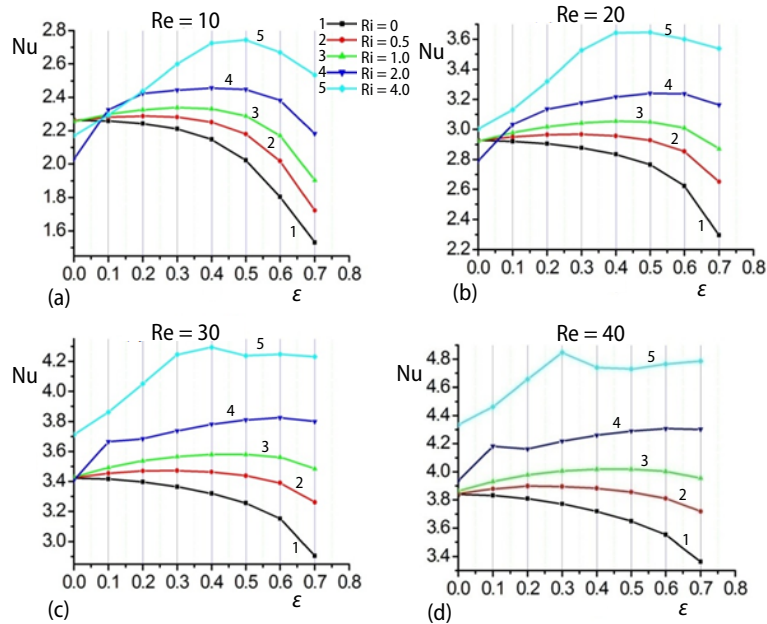


Figure 12. Effect of ε , Ri , and Re on average Nusselt number
 (for color image see journal web site)

$Pr = 1$. As shown in fig. 12, the average Nusselt number increases as usual with the Reynolds number for all Richardson number due to the gradual thinning of thermal boundary-layers with increasing Reynolds number. However, at $\varepsilon = 0$ the influence of Richardson number on Nusselt number gradually increases with a progressive increase in Reynolds number. For forced convection ($Ri = 0$) increase in the eccentricity factor decreases the heat transfer rate for all Reynolds number due to the decrease of local Reynolds number, which decreases thinning of thermal boundary-layer. Interesting variations are observed with respect to the eccentricity factor, for $0 < Ri \leq 4$, increase in ε promotes the heat transfer rate, reaches to the maximum value at certain value ε and then again decreases for example a change in ε from 0 to 0.5 increases Nusselt number by 22% for $Ri = 4$, at $Re = 10$. It is due to the increment of flow rate over the cylinder which increases thinning of thermal boundary-layer. Furthermore, in fig. 12 the influence of ε on the average Nusselt number gradually increases with a progressive increase in Richardson number.

Conclusions

The numerical study of the effects of eccentricity factor $0 \leq \varepsilon \leq 0.7$, and thermal buoyancy $0 \leq Ri \leq 4$ on the flow field and heat transfer characteristics of Newtonian fluid around a circular cylinder confined in 2-D channel for steady flow regime ($10 \leq Re \leq 40$). The main results are summarized as follow.

- The dimensionless length of both vortices decreases with increase in the value of Richardson number, and they vanish at all when Richardson number reaches the critical value
- From $Ri = 1-4$ at $\varepsilon = 0$ two re-circulation zone appear over the cylinder and on the down wall of channel behind the cylinder, and they increase in both directions longitudinal and lateral by increasing Re and/or Ri
- From $\varepsilon = 0-0.7$ with increasing ε , the above wake diminishes progressively, and at some value of ε , it is suppressed at all above the cylinder. On the other hand, the down wake increases initially and then decreases.
- At $Ri = 0$, both of C_D and Nusselt number decrease with increasing in the value of eccentricity factor
- At $\varepsilon = 0$, increase Richardson number over 1 decreases the heat transfer rate
- Increase in value of ε increases the Nusselt number initially, and then decreases.
- The influence of ε on the average Nusselt number gradually increases with a progressive increase in Richardson number.
- An increase in eccentricity factor from 0 to 0.3 increases C_D by 37% at $Re = 10$, and 30% at $Re = 20$ for $Ri = 4$.
- An increase in eccentricity factor form 0 to 0.4 increases Nusselt number by 20.4% at $Re = 10$, and 18.6% at $Re = 30$ for $Ri = 4$.

Nomenclature

| | |
|---|---|
| B – blockage ratio, ($= d/H$) | L_d – downstream distance, [m] |
| C_D – drag coefficient, [-] | L_u – upstream distance, [m] |
| d – cylinder size, [m] | L_R – dimensionless re-circulation length, [-] |
| e – distance between centers of channel and cylinder, [m] | Nu – local Nusselt number, ($= hd/k$), [-] |
| Gr – Grashof number, ($= g\beta(T_w - T_m)d^3/\eta^2$), [-] | n_s – normal direction, [-] |
| g – acceleration due to gravity, [ms^{-2}] | Pr – Prandtl number, ($= h/a$), [-] |
| H – height of computational domain, [m] | p – dimensionless pressure, ($= \bar{p}/\rho u_{max}^2$), [-] |
| h – local heat transfer coefficient, [Wm^2K^{-1}] | Re – Reynolds number, ($= u_{max}d/\nu$), [-] |
| k – thermal conductivity of fluid, [$Wm^{-1}K^{-1}$] | Ri – Richardson number, ($= Gr/Re^2$), [-] |
| | T – temperature, [K] |

| | |
|--|---|
| T_w – cylinder temperature, [K] | β – coefficient of volume expansion, [K ⁻¹] |
| T_{in} – inlet temperature, [K] | ε – eccentricity factor |
| u_{max} – maximum velocity profile, [ms ⁻¹] | ν – kinematic viscosity of fluid, [m ² s ⁻¹] |
| u – dimensionless axial velocity, ($= \bar{u}/u_{max}$), [-] | θ – dimensionless temperature, [$= (T - T_{in})/(T_w - T_{in})$], [-] |
| v – dimensionless normal velocity, ($= \bar{v}/u_{max}$), [-] | ρ – density of the fluid, [kgm ⁻³] |
| x – dimensionless axial co-ordinate, ($= \bar{x}/d$), [-] | Subscript |
| y – dimensionless normal co-ordinate, ($= \bar{y}/d$), [-] | max– maximum |
| Greek symbols | Superscript |
| α – thermal diffusivity of the fluid, [m ² s ⁻¹] | – – dimensional quantity |

References

- [1] Ribeiro, V. M., *et al.*, Viscoelastic Fluid Flow Past a Confined Cylinder: Three-Dimensional Effects and Stability, *Chemical Engineering Science*, 111 (2014), May, pp.364-380
- [2] Valipour, M. S., *et al.*, A Numerical Study on Convection around a Square Cylinder Using Al₂O₃-H₂O Nanofluid, *Thermal Science*, 18 (2014), 4, pp. 1305-1314
- [3] Dhiman, A. K., *et al.*, Steady Flow Across a Confined Square Cylinder: Effects of Power-Law Index and Blockage Ratio, *J. Non-Newtonian Fluid Mech.*, 148 (2008), 1-3, pp. 141-150
- [4] Greenblatt, D., Wagnanski, I. J., The Control of Flow Separation by Periodic Excitation, *Prog. Aerosp. Sci.*, 36 (2000), 7, pp. 487-545
- [5] Chatterjee, D., Raja, M., Mixed Convection Heat Transfer Past In-Line Square Cylinder in Vertical Duct, *Thermal Science*, 17 (2013), 2, pp. 567-580
- [6] Sasmal, C., Chhabra, R. P., Effect of Aspect Ratio on Natural Convection in Power-Law Liquids from a Heated Horizontal Elliptic Cylinder, *Int. J. of Heat and Mass Transfer*, 55 (2012), 17-18, pp. 4886-4899
- [7] Mohammed, H. A., Salman, Y. S., Numerical Study of Combined Convection Heat Transfer for Thermally Developing upward Flow in Vertical Cylinder, *Thermal Science*, 12 (2008), 2, pp. 89-102
- [8] Nirmalkar, N., Chhabra, R. P., Forced Convection in Power-Law Fluids from an Asymmetrically Confined Heated Circular Cylinder, *In. J. of Heat and Mass Transfer*, 55 (2012), 1-3, pp. 235-250
- [9] Lin, Y. M., Wu, G. H., *et al.*, Non-Isothermal Flow of a Polymeric Liquid Passing an Asymmetrically Confined Cylinder, *In. J. of Heat and Mass Transfer*, 47 (2004), 8-9, pp. 1989-1996
- [10] Subbarao, A., *et al.*, Modelling Laminar Transport Phenomena in a Casson Rheological Fluid from an Isothermal Sphere with Partial Slip, *Thermal Science*, 19 (2015), 5, pp. 1507-1519
- [11] Chatterjee, D., Mondal, B., Forced Convection Heat Transfer from an Equilateral Triangular Cylinder at Low Reynolds Numbers, *Heat Mass Transfer*, 48 (2012), 9, pp. 1575-1587
- [12] Chandra, A., Chhabra, R. P., Flow and Forced Convection Heat Transfer in Newtonian Fluids from a Semi-Circular Cylinder, *International Journal of Heat and Mass Transfer*, 54 (2011), 1-3, pp. 225-241
- [13] Taymaz, I., *et al.*, Numerical Investigation of Incompressible Fluid Flow and Heat Transfer around a Bluff Bodies in Channel, *Thermal Science*, 19 (2015), 2, pp. 537-547
- [14] Jahromi, J. A., *et al.*, Effects of Inclination Angle on the Steady Flow and Heat Transfer of Power-Law Fluids around a Heated Inclined Square Cylinder in a Plane Channel, *J. of Non-Newtonian Fluid Mechanics*, 166 (2011), 23-24, pp. 1406-1414
- [15] Soares, A. A., Ferreira, J. M., Effect of Temperature-Dependent Viscosity on Forced Convection Heat Transfer from a Cylinder in Cross Flow of Power-Law Fluids, *Int. J. of Heat and Mass Transfer*, 53 (2010), 21-22, pp. 4728-4740
- [16] Krishnan, S., Aravamudan, K., Simulation of Non-Newtonian Fluid Food Particle Heat Transfer in the Holding Tube Used in Aseptic Processing Operations, *Food and Bioproducts Processing*, 9 (2013), 1, pp. 129-148
- [17] Rashidi, S., *et al.*, Structural Optimization of Nanofluid Flow around an Equilateral Triangular Obstacle, *Energy*, 88 (2015), Aug., pp. 385-398
- [18] Rashidi, S., Esfahani, J. A., The Effect of Magnetic Field on Instabilities of Heat Transfer from an Obstacle in a Channel, *Journal of Magnetism and Magnetic Materials*, 391 (2015), Oct., pp. 5-11
- [19] Bovand, M., *et al.*, Enhancement of Heat Transfer by Nanofluids and Orientations of the Equilateral Triangular Obstacle, *Energy Conversion and Management*, 97 (2015), June, pp. 212-223

- [20] Merkin, J. H., Mixed Convection from a Horizontal Circular Cylinder, *Int. J. Heat Mass Transfer*, 20 (1977), 1, pp. 73-77
- [21] Sarkar, A., *et al.*, Unsteady Wake Dynamics and Heat Transfer in Forced and Mixed Convection Past a Circular Cylinder in Cross Flow for High Prandtl Numbers, *J. of Heat and Mass Transfer*, 54 (2011), 15-16, pp. 3536-3551
- [22] Sukesan, M. K., Dhiman, A. K., Laminar Mixed Convection in a Chanel with a Build-In Semi-Circular Cylinder under the Effect of Cross-Buoyancy, *International Communications in Heat and Mass Transfer*, 58 (2014), Nov., pp. 25-32
- [23] Chatterjee, D., Amiroudine, S., Two-Dimensional Mixed Convection Heat Transfer from Confined Tandem Square Cylinder in Cross-Flow at Low Reynolds Number, *International Communications in Heat and Mass Transfer*, 37 (2010), 1, pp. 7-16